JOURNAL OF THERMOPHYSICS AND HEAT TRANSFER
Vol. 23, No. 3, July–September 2009

Significance of Nonequilibrium Surface Interactions in Stardust Return Capsule Ablation Modeling

A. F. Beerman* and M. J. Lewis†
University of Maryland, College Park, Maryland 20742
R. P. Starkey‡
University of Colorado, Boulder, Colorado 80309
and
B. Z. Cybyk§
Johns Hopkins University Applied Physics Laboratory, Laurel, Maryland 20732

DOI: 10.2514/1.38863

The gas-surface modeling of high-density materials exposed to high-pressure atmospheric reentry conditions was extended to include low-density materials interacting with low-pressure atmospheric conditions. The fully implicit ablation thermal response code and multicomponent ablation thermochemistry program were extended to include nonequilibrium surface conditions for the Stardust return capsule. The Stardust return capsule reentered Earth's atmosphere experiencing low pressure and had a low-density heat shield material. The material response of the Stardust return capsule was previously only modeled with surface equilibrium. Validation against Stardust reentry flight data showed that the equilibrium assumption led to an overprediction of recession and that the inclusion of nonequilibrium reduced the overprediction of this parameter. Incorporating the Park finite rate model nonequilibrium surface conditions led to a reduction in the calculated value of recession at the stagnation point from 1.12 to 0.72 cm in a nominal simulation of the Stardust return capsule. The nonequilibrium recession was closer to the measured recession of 0.65 cm. Incorporating nonequilibrium conditions also decreased the calculated total heat load from 28 to 19 kJ/cm^2. The improved material response method is applicable to a range of reentries, including future missions such as the Orion crew exploration vehicle.

Nomenclature

B	=	preexponential factor, s^{-1}
B'	=	dimensionless mass blowing rate, $\dot{m}/\rho_e u_e C_M$
C_H	=	Stanton number for heat transfer
C_i	=	mass fraction for species i
C_M	=	Stanton number for mass transfer
c_p	=	specific heat, J/kg-K
D_i	=	diffusion coefficient for species i, m^2/s
E	=	activation temperature, K
F	=	view factor
H_r	=	recovery enthalpy, J/kg
h	=	enthalpy, J/kg
$\bar{h}$	=	partial heat of charring, J/kg
k	=	Boltzmann constant, J/K
M	=	molecular weight, kg/mole
m	=	mass, kg
$\dot{m}$	=	mass flux, kg/m^2 s
p	=	pressure, N/m^2
q_c	=	conductive heat flux, W/m^2
q_{rad}	=	radiative heat flux, W/m^2
T	=	temperature, K
u	=	velocity, m/s
v_w	=	mass injection velocity, m/s
x	=	moving coordinate system, $y - s$, m
Y	=	element mass fraction
y	=	stationary coordinate, m
α	=	surface absorption
β	=	efficiency of gas-surface interaction
Γ	=	volume faction of resin
ε	=	surface emissivity
λ	=	blowing reduction parameter
ρ	=	density, kg/m^3
σ	=	Stefan–Boltzmann constant, W/m^2 K^4
ψ	=	decomposition reaction order

Subscripts

c	=	char
d	=	density component
e	=	boundary-layer edge
g	=	pyrolysis gas
i	=	surface species
k	=	element or gaseous base species
s	=	surface
v	=	original
w	=	wall

Presented as Paper 1224 at the 46th AIAA Aerospace Sciences Meeting and Exhibit, Reno, NV, 7–10 January 2008; received 31 May 2008; revision received 30 April 2009; accepted for publication 3 May 2009.

*Graduate Research Assistant, Department of Aerospace Engineering, 3181 Glenn L. Martin Hall; abeerman@umd.edu. Student Member AIAA.

†Professor, Department of Aerospace Engineering, 3181 Glenn L. Martin Hall; mjlewis@umd.edu. Fellow AIAA.

‡Assistant Professor, Department of Aerospace Engineering Sciences; rstarkey@colorado.edu. Senior Member AIAA.

§Assistant Group Supervisor, Global Engagement Department, 11100 Johns Hopkins Road; bohdan.cybyk@jhuapl.edu. Associate Fellow AIAA.

I. Introduction

THERMOCHEMICAL ablation may occur on surfaces as a result of high heat transfer associated with hypersonic flight, particularly during the atmospheric entry of a space vehicle. Heat shields must be designed to take the brunt of the energy encountered during the reentry portion of a spacecraft trajectory. Because the effects of ablation must be considered when sizing the heat shield, understanding hypersonic flow and ablation is critical to the development of heat shields.

Nonequilibrium chemical effects may affect the aerodynamic performance of a heat shield [1]. Park reviewed analysis of the response of the heat shield surface during the reentry of Apollo missions and determined that the surface may not have reached chemical equilibrium [2]. Previous to that work, assumptions of equilibrium likely led to an overprediction of the heat fluxes on the surface of the Apollo capsule. Park modified the previously used Apollo model to account for nonequilibrium surface interactions and generated results that more closely matched those on the actual Apollo capsule. Further applications of a nonequilibrium assumption for surface interactions on the Pioneer–Venus probes and Galileo entry probe produced results similar to their respective flight-test data [2]. Nonequilibrium effects may appear in a model due to the physical properties of a heat shield. The Apollo missions used a carbon-silicon carbide heat shield; the Pioneer–Venus probes and Galileo entry probe used carbon phenolic for their heat shield. In the present work, nonequilibrium surface interactions are applied to a phenolic-impregnated carbon ablator (PICA) [3], using the Stardust mission as the computational base. PICA is a relatively new heat shield ablator, and the reaction set associated with a PICA heat shield interacting with the surrounding gas flow may differ from other types of heat shields.

The Stardust return capsule (SRC) had the highest entry velocity of any Earth entry vehicle, 12.8 km/s. In contrast, the fastest Apollo capsule, the unmanned Apollo 4, returned with a speed of 11.0 km/s. A comparison of the SRC computational models with the SRC flight-test data revealed that the computational models used to predict such parameters as recession and temperature on the SRC had overpredicted those values, sometimes by more than 50% [4]. The computational models used to generate the predicted data took into account nonequilibrium flow conditions, but assumed equilibrium at the surface. In a previous work, nonequilibrium surface conditions were applied at the stagnation point across the entire Stardust trajectory [5]. That analysis focused on only one type of reaction in a finite rate ablation model and was compared against limited data from the SRC reentry. In the present work, the nonequilibrium analysis has been expanded to two reactions and is compared against additional Stardust reentry data.

Various studies by Park and Ahn [6], Park [7], and Chen and Milos [8] have examined nonequilibrium surface interactions on heat shields reentering the Earth's or other planets' atmospheres; however, these efforts typically have not extended the models in those studies to compute ablation. Park derived a numerical model [7] for the Stardust return capsule that used finite rate ablation to calculate the species concentrations on the surface, with a reaction set that included sublimation, nitridation, and one oxidation reaction. The convective heat fluxes were calculated with and without radiation, and the total mass injection rates from the equilibrium analysis of the SRC by Olynick et al. [9] were used to account for total ablation and the pyrolysis gas rate. Park held the total ablation rate constant and computed the pyrolysis gas rate using that total value. The present work uses a similar approach by computing the pyrolysis gas rate and char ablation rate individually to find the total mass injection (total ablation) rate. The objective is to develop a model that can predict both equilibrium and nonequilibrium surface effects in the calculation of material response. In the present work, nonequilibrium surface reactions were applied to a low-density heat shield encountering a low-pressure reentry trajectory similar to that encountered by the Stardust return capsule.

The fully implicit ablation thermal (FIAT) response program [10] was used as the material response model. The FIAT program typically assumes chemical equilibrium at the surface; however, in the current work, nonequilibrium surface models are applied using the multicomponent ablative thermochemistry (MAT) code [11]. The capabilities of MAT were extended to include nonequilibrium effects that were input into FIAT. This new implementation created a material response model that accounts for possible nonequilibrium surface conditions that may occur during reentry. The main focus of this paper is to describe the new implementation process and to provide some results relevant to the SRC and future spacecraft, including NASA's crew exploration vehicle (CEV).

II. Background

A. Stardust Return Capsule

The Stardust return capsule used a PICA [10] for its heat shield, a relatively low-density material also selected for NASA's CEV. PICA was developed in the mid-1990s, and there has recently been an increase in arcjet testing and associated data due to its selection as the heat shield material for the CEV. The Stardust heat shield also was constructed with a sandwichlike structure of aluminum honeycomb and faceplates made of graphite polycyanate. The Stardust return capsule was recovered on 16 January 2006.

The first 100 s of its nominal reentry trajectory, as defined by Olynick et al. [9], are presented in Fig. 1. Kontinos and Stackpoole [4] determined that the actual trajectory closely followed the nominal trajectory. A DC-8 flown at an altitude of 11.9 km was used as an airborne observatory to optically determine average surface temperature [12]. Because the capsule was not fully instrumented to measure reentry conditions, Jenniskens [13] used an echelle spectroscope to observe the flow around the capsule as it returned to Earth. Postflight analysis determined surface temperature and recession. The observed data suggested that the previous Stardust models were inaccurate; recession was overpredicted by 50% at some locations on the capsule [14].

B. Heat Shield Material Selection

Heat shield surface reactions are dependent on the material composition. The bonds between the atoms that compose a heat shield dictate how it will react during extreme conditions. In a typical reentry, there is a period of particularly intense heating, with the magnitude and duration depending on the trajectory. During this time, the heat shield material decomposes most rapidly. The ablative reactions for carbonaceous materials result in the production of decomposition gases and solid carbonaceous char residue [15]. In a carbonaceous heat shield, the char layer resulting from ablation can vaporize through sublimation or oxidation or combine with atomic nitrogen to form CN. The pyrolysis gas and the vapor from the char layer are injected into the flow [15]. Apollo data showed that, for steady-state ablation, the mass ratio between the pyrolysis gas and the gaseous carbon is not the same as the mass ratio of the components of the original material [16]. When charring occurres, such as during the Apollo missions, heat shield ablation generates char and pyrolysis gas with dissimilar compositions. The porous residual char that remains after ablation has a lower density than the original solid and different thermal and structural properties [17].

PICA is an example of an ablation material that is made up of carbon and phenolic [3]. PICA consists of a low-density, preformed carbon fiber substrate and is constructed using a unique infiltration technique to place the phenolic resin inside the carbon. The uniqueness of the infiltration technique results in a lower density for PICA compared with other carbon-phenolic materials. The carbon fiber insulation of PICA has an initial density between 0.152 and 0.176 g/cm^3, with the overall density falling in the range of 0.224–0.248 g/cm^3. This overall density is 4–8 times lower than more-conventional carbon phenolics. In general, the reactions that occur on the surface of PICA, as with other carbon materials [18], can

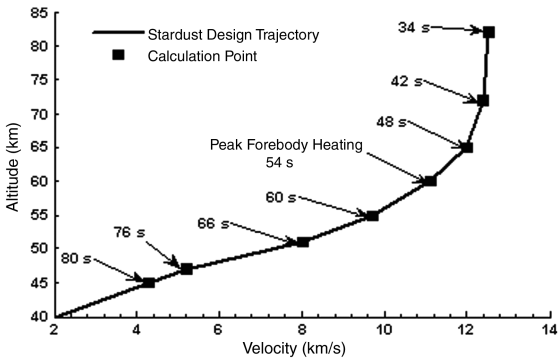

Fig. 1 Nominal Stardust reentry trajectory.

be divided into three regimes: rate-controlled oxidation, diffusion-controlled oxidation, and sublimation [3]. Arcjet testing by Covington et al. [19] at heating rates of 1150 and 1630 W/cm^2 found that diffusion-controlled recession occurs in PICA under those conditions.

C. Surface Interactions: Park Finite Rate Model

Park derived a finite rate gas-surface interaction model that accounts for nonequilibrium surface interactions, including oxidation [Eqs. (1) and (2)], nitridation [Eq. (3)], and sublimation of the carbon [Eq. (4)] [6,7,20]:

$$\dot{m}_1 = \rho C_O \bar{v}_O \beta_O (M_C/M_O) \tag{1a}$$

$$O + C_{(s)} \rightarrow CO \tag{1b}$$

$$\dot{m}_2 = 2\rho C_{O2} \bar{v}_{O2} \beta_{O2} (M_C/M_{O2}) \tag{2a}$$

$$O_2 + C_{(s)} \rightarrow 2CO \tag{2b}$$

$$\dot{m}_3 = \rho C_N \bar{v}_N \beta_N (M_C/M_N) \tag{3a}$$

$$N + C_{(s)} \rightarrow CN \tag{3b}$$

$$\dot{m}_4 = \rho (C_{C3,E} - C_{C3}) \bar{v}_{C3} \beta_{C3} \tag{4a}$$

$$3C_{(s)} \rightarrow C_3 \tag{4b}$$

$$\dot{m}_c = \dot{m}_1 + \dot{m}_2 + \dot{m}_3 + \dot{m}_4 = \rho_s \dot{S} \tag{5}$$

The mean molecular speed, $\bar{v}_i$, for each species i is defined as $\sqrt{kT_W/2\pi m_i}$. As per Eq. (4), sublimation produces primarily C_3 in this model [8]. In the Park model, the mass loss due to charring is the sum of the four reactions' mass fluxes [Eq. (5)].

In a Park finite rate model without inputs from a material response program, species mass conservation at the surface is written as [8]

$$-\rho D_i \nabla X_i + \rho v_w C_i = \hat{N}_i + \dot{m}_g C_{i,g} \tag{6}$$

The mass transfer through diffusion and convection are the first and second terms on the left, respectively. $\hat{N}_i$ is the source term and, for the CO, CN, C_3, N, O, and O_2 species, they are as follows [8]:

$$\hat{N}_{CO} = \dot{m}_1 (M_{CO}/M_C) + \dot{m}_2 (M_{CO}/M_C)$$
$$\hat{N}_{CN} = \dot{m}_3 (M_{CN}/M_C), \qquad \hat{N}_{C_3} = \dot{m}_4 \qquad \hat{N}_N = -\dot{m}_3 (M_N/M_C)$$
$$\hat{N}_O = -\dot{m}_1 (M_O/M_C), \qquad \hat{N}_{O_2} = -\dot{m}_2 (M_{O_2}/2M_C) \tag{7}$$

For all the other species, the source term is zero.

The total mass blowing based on the global mass balance is

$$\rho v_w = \dot{m}_c + \dot{m}_g \tag{8}$$

where ρ is the total gas density. Park's model assumes that the reaction rates are negligibly small for both the oxygen atom and nitrogen atom recombination:

$$O + O \rightarrow O_2 + 5.08 \text{ ev} \tag{9}$$

$$N + N \rightarrow N_2 + 9.8 \text{ ev} \tag{10}$$

Park assumed small surface catalysis for these reactions because their effects were not significant in various experiments [7]. However, the absence of surface recombination may lead to lower convective heating when compared with a fully catalytic wall if these reactions are not accounted for elsewhere in a surface reaction model.

Equation (6) is nonlinear but can be solved iteratively. The surface temperature, pyrolysis gas injection rate, and species concentrations of pyrolysis gas must be specified so that the species concentration and the velocity can be updated. Chen and Milos [8] assumed that the gas injected into the flow is in chemical equilibrium and ablation is steady state. These assumptions decoupled the surface temperature and pyrolysis gas injection rate. The method discussed in the current work builds upon this effort, but uses FIAT and MAT to provide the surface temperatures and species concentration for the Park finite rate model.

III. Numerical Methods of Computational Models

A. Fully Implicit Ablation Thermal Material Response Model

Previous researchers have used the charring material ablation (CMA) code for thermal protection sizing [10,21]. The CMA code solves the internal energy balance and decomposition equations coupled with the ablating surface energy balance condition [22]. This code was implemented using an explicit algorithmic formulation and can be highly sensitive to spatial and temporal resolution [10]. In contrast, FIAT does not have this sensitivity. FIAT computes the transient one-dimensional thermal response of thermal protection system materials arranged in a multilayer stack up, subject to aerothermal heating on one surface, and can be coupled to a computational fluid dynamics flow solver. The FIAT code is described in [10].

In the present work, heating is predicted using a boundary condition that includes convection, radiation flux across the surface, heating due to chemistry, and conduction:

$$C_H(H_R - (1 + B')h_w) + \dot{m}_g h_g + \dot{m}_c h_c + q_{\text{rad}} - F\sigma\varepsilon_w T_w^4 - q_{\text{cond}} = 0 \tag{11}$$

where C_H is the blown heat transfer coefficient and H_R is the recovery enthalpy. If the material is ablating, the blown heat transfer coefficient is derived from the corrected form of the unblown heat transfer coefficient, C_{H1}:

$$\frac{C_H}{C_{H1}} = \frac{2\lambda B'}{\exp(2\lambda B') - 1} = \frac{\ell_n(1 + 2\lambda B')}{2\lambda B'} \tag{12}$$

where

$$B'_1 = \dot{m}/C_{H1}, \qquad B' = \dot{m}/C_H$$

In the case of a nonablating material, the unblown heat transfer coefficient is used in calculations. The addition of nonequilibrium surface conditions in this work affected the calculation of the B' parameter employed in Eq. (12).

B. Multicomponent Ablative Thermochemistry Surface Interactions with Nonequilibrium

In the current effort, the surface chemistry inputs are provided to FIAT by an interface with MAT. Note than an early version of MAT originally included oxidation nonequilibrium reactions [11], but the current version considers only equilibrium. With the earlier nonequilibrium capability, carbon dioxide and nitrogen species surface reactions were considered to be in full equilibrium because they were slower than the oxidation reactions. Reactions involving sublimation and nitridation were also kept in full equilibrium. MAT modeled these chemical reactions as a conversion of one

pseudoelement in a condensed reactant species into another element of the same atomic weight in one of the product species. MAT originally could alternate between two early kinetic models (Park [23] and Scala [24]) in its calculation of nonequilibrium surface reaction rates. The model proposed by Park [23] attempted to update a semi-empirical formula that described ablation rates of commercial grade graphites. This formula was not applicable to low-density flows in which oxidation may occur. Park used reaction probability to improve upon the semi-empirical model, which generally led to a higher predicted ablation rate and greater mass loss value. Park's method is also more applicable to low dynamic pressures. The current work has the original nonequilibrium capability in MAT integrated back into the program, but replaces the earlier models with an expanded finite rate model proposed by Park that contains oxidation and additional reactions [6,7,20].

The equilibrium element conversion equation used in MAT is [25]

$$\dot{m}_g Y_{kg} + \dot{m}_c Y_{kc} = j_{kw} + (\rho v)_w Y_{kw} \tag{13}$$

When summed over the base species index k, this becomes

$$\dot{m}_g + \dot{m}_c = \sum_k j_{kw} + (\rho v)_w \tag{14}$$

In standard usage, the diffusional fluxes, j_{kw}, are obtained by the transfer potential method, such that [25]

$$j_{kw} \approx \rho_e u_e C_M (Z^*_{kw} - Z^*_{ke}) \tag{15}$$

The diffusion-coefficient–weighted average of the mass and mole fractions is represented by the variable Z^* [26]. By assuming that the diffusion coefficients are equal, Z^* and Y can be made equivalent. The equilibrium element flux balance can be found using Eqs. (13–15):

$$Y_{kw} = \frac{Y_{ke} + B'_g Y_{kg} + B'_c Y_{kc}}{1 + B'_g + B'_c} \tag{16}$$

Because the mass fraction, Y_{kw}, must be between 0 and 1, it sets a bound on both the numerator and denominator of Eq. (16). B'_c and B'_g are often specified as independent parameters. B'_c is the dimensionless char ablation rate, and B'_g is the dimensionless pyrolysis gas rate. These dimensionless terms come from non-dimensionalizing the char or pyrolysis mass flux by the mass transfer coefficient. The heat transfer coefficient at the previously determined peak heating point for the Stardust trajectory (54 s) was used to nondimensionalize the mass fluxes. The pressure and dimensionless char and pyrolysis gas ablation rates can be user-defined in MAT. The mass transfer coefficient, C_M, is related [27] to the heat transfer coefficient C_H through the Lewis number, Le: $C_M = C_H Le^{2/3}$. Both MAT and FIAT assume the Lewis number is equal to 1.

Equation (17) is the element flux balance equation that takes into account the nonequilibrium reaction mass flux [11]:

$$Y_{kw} = \frac{Y_{ke} + B'_g Y_{kg} + B'_c Y_{kc} - B'_{kr}}{1 + B'_g + B'_c} \tag{17}$$

The temperature and the enthalpy at the wall are functions of B'_c, B'_g, and the pressure. The finite rate reactions must be accounted for when their elemental components are called upon in Eqs. (16) and (17). B'_{kr} is the result of modeling chemical reactions as a conversion of one pseudoelement into another element [11]. Park's model only affects the species created by the reactions defined in Eqs. (1–4), as those are the only reactions that determine the value of B'_{kr}. All other reactions take place as if they were reaching equilibrium. Recombination of oxygen and nitrogen is allowed to occur as if in equilibrium, and the surface is fully catalytic.

IV. Finite Rate Ablation Results on a Nominal Trajectory

Heating and recession values were calculated at the stagnation point on a heat shield with SRC geometry across a nominal trajectory. A baseline equilibrium case is generated for a 750 s trajectory, with inputs derived from [10] for the trajectory path outlined in Fig. 1. The computed baseline equilibrium case matches the results found by Olynick [9]. The calculated equilibrium heat fluxes are presented in Fig. 2. The radiative heat flux, that is, the radiation entering the material from the surroundings, is an input parameter taken directly from [10]. Figure 3 provides a side-by-side comparison of the mass flux due to char and pyrolysis gas. The total surface recession is 1.12 cm, or about one-sixth of the original thickness (6.45 cm) of the heat shield. When assuming equilibrium surface interactions, the majority of original material loss occurs due to char ablation.

A. Analysis of the Effects of Nitridation

Nonequilibrium conditions, both with and without nitridation, are calculated using Park's model. The computed nonequilibrium reentry data are compared with data calculated using equilibrium conditions. Chen and Milos studied the effect of finite rate nitridation in their use of the Park finite rate model [8]. In the present work, the same approach is taken and incorporated into MAT. Nonequilibrium surface interactions are applied to the entire trajectory; however, nonequilibrium is important only when the surface temperature reaches some threshold, which may occur at only a few points on the trajectory. The removal of nitridation from the Park model means that it is being modeled in MAT as occurring in equilibrium and not as a finite rate reaction. Analysis of the material response for both the full reaction set and the reaction set without nitridation shows that the removal of nitridation has an effect on the nonequilibrium condition of, at the most, a few percentage points in the recession calculation and other calculated parameters. Nitridation essentially reaches an equilibrium state on the surface even when a finite rate model is employed. The differences between the two conditions are negligible and the full reaction set was chosen as the baseline nonequilibrium

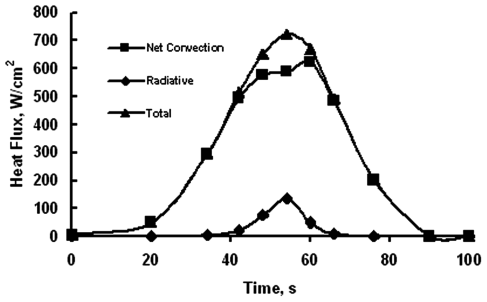

Fig. 2 Calculated heat fluxes at the Stardust stagnation point versus time.

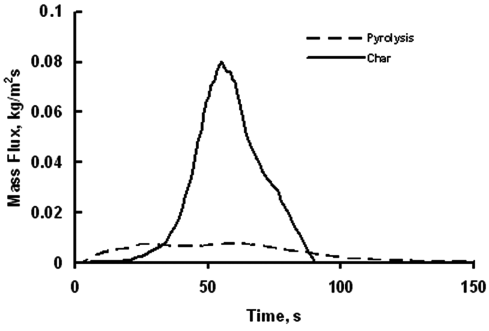

Fig. 3 Calculated stagnation point equilibrium mass flux rates versus time for the Stardust aeroshell.

case due to its completeness. A complete comparison between the full reaction set and the nitridation-absent case can be found in [5].

Calculated nonequilibrium temperatures remain close to those computed with equilibrium conditions for the chosen trajectory. The surface temperature decreases from a peak of 3370 K at 54 s to a peak of 3150 K at 55 s, a change of 6.5%. Figure 4 shows the char ablation computed by FIAT for the full reaction set of Park's model applied to Stardust reentry compared with the equilibrium case. The rate at which ablation occurs is lower under nonequilibrium conditions. At the peak ablation rate, roughly 60 s, finite rate ablation results in a computed loss of char at the rate of 0.049 kg/m^2s. This is a decrease of 39% from a peak char ablation rate of 0.080 kg/m^2s in the equilibrium calculation.

The net convective heat flux is described by the following expression:

$$C_H(H_r - h_w) \tag{18}$$

The magnitude of the blown heat transfer coefficient depends on the total ablation rate; thus, the net convective heat flux also depends on that rate. If B' (which is the nondimensional form of the total ablation rate) decreases due to a decrease in the char ablation rate, then the ratio of C_H/C_{H1} increases. If the other parameters remain constant, the computed net convective heat flux increases. However, the enthalpy at the wall is greater in the presence of finite rate ablation, offsetting the calculated increase in the blown heat transfer coefficient. The net result is a decrease in the net convective heat flux under nonequilibrium conditions (Fig. 5). Oxygen and nitrogen recombination are kept fully catalytic, and so their absence in the finite rate model does not affect the convective heat flux.

The radiative heat flux is the same in both the equilibrium and nonequilibrium cases. The maximum nonequilibrium net convective heat flux, 460 W/cm^2, occurs at 48 s, 12 s earlier than in the equilibrium model. The peak total heat flux using the Park finite rate model occurs at the same time as the peak in equilibrium, 54 s, and is 580 W/cm^2 (a decrease of 19% from the equilibrium analysis). The decrease in the convective heat flux leads to a decrease in the convective heat load and the total heat load encountered by the PICA material. The maximum total nonequilibrium heat load (Fig. 6) is 19 kJ/cm^2, a decrease of 32% from the equilibrium case. The radiative heat load contributes 9.7% of the total heat load, an increase of 6.4% in the equilibrium calculation. The surface recession is reduced 36%, from 1.12 to 0.72 cm. In the nonequilibrium calculation, convective effects decrease and so radiative heating is relatively more important than in an equilibrium calculation.

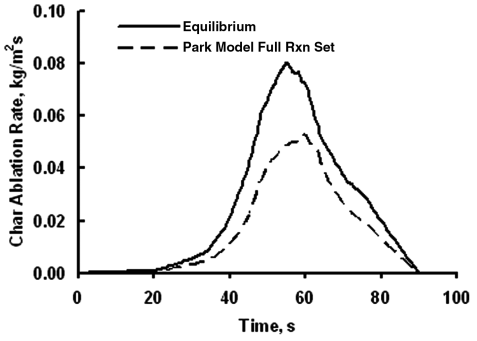

Fig. 4 Computed char ablation rate versus time for Park's model [8] using the full reaction set.

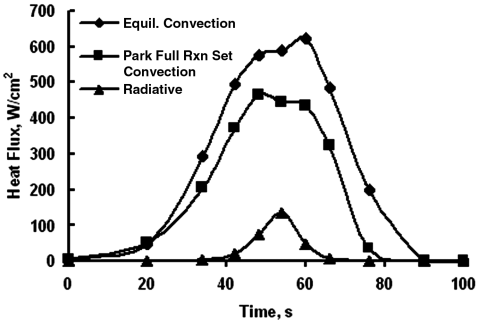

Fig. 5 Computed heat fluxes for the equilibrium model [10] and Park finite rate model [8] versus time.

B. Analysis of the Effects of Sublimation

The Park finite rate model includes four reactions that can be isolated to study their individual effects. Previous work showed that nitridation can be eliminated with minimal impact [5]. In the present work, the effect of eliminating sublimation, an important reaction when temperatures are over 3000 K, is studied. Sublimation and nitridation are removed from the Park finite rate model reaction set; the two oxidation reactions are the only finite rate nonequilibrium reactions.

Without sublimation there is a sharp drop-off in the surface temperature after 54 s. Sublimation is an endothermic reaction on the surface. Removing sublimation from the Park model allows the sublimation reaction to act in an equilibrium manner within MAT and to fully cool the surface. In the absence of finite rate sublimation, the surface cools more quickly and reaches a lower temperature when compared with the previous cases of equilibrium and nonequilibrium without nitridation (Fig. 7). Overall, the absence of finite rate sublimation has a minimal impact for the first 54 s of the trajectory before the surface reaches a temperature at which sublimation is likely to occur. The steady-state temperature that the surface eventually reaches for nonequilibrium without sublimation is only a few tens of Kelvin lower than the temperatures for nonequilibrium with sublimation. Thus, sublimation is important in the reaction set only when it is activated.

The char ablation rate without finite rate sublimation diverges from the previous nonequilibrium results at 54 s, as seen in Fig. 8. The char ablation rate reaches a peak of 0.047 kg/m^2s, compared with 0.080 kg/m^2s for equilibrium surface conditions. It then decreases to 0.018 kg/m^2s around 70 s before rapidly decreasing. The char ablation rate decreases because C_3 is not forming. The new recession without sublimation is 0.49 cm, which is lower than the

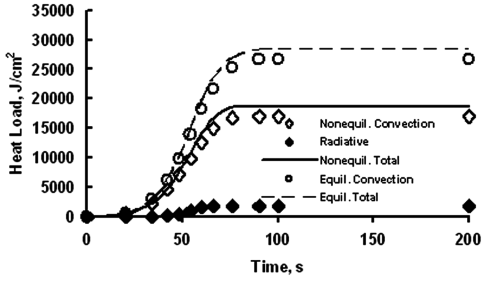

Fig. 6 Calculated heat loads for the full Park finite rate model [8] and the equilibrium model [10] versus time.

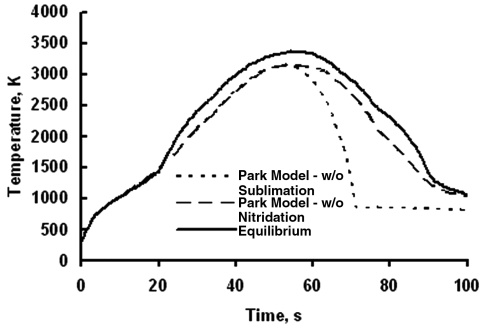

Fig. 7 Predicted SRC surface temperature profile for the three surface interaction models [8,10] versus time.

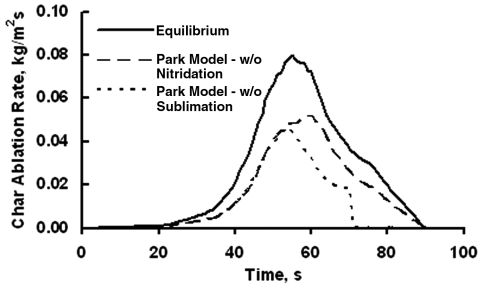

Fig. 8 Calculated char ablation rate versus time for the three surface conditions [8,10].

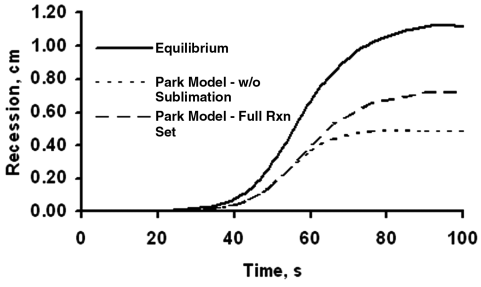

Fig. 9 Recession profile predicted by FIAT for the three models [8,10].

recession computed for full nonequilibrium and equilibrium (Fig. 9). Beyond the peak heating at 54 s, sublimation dominates the finite rate ablation model. Park's analysis of equilibrium and nonequilibrium surface interactions on the Apollo heat shield showed that nonequilibrium and equilibrium surface interactions should generate similar trends [1]. When nonequilibrium without finite rate sublimation is calculated, the char ablation and surface temperature trends do not match those found in the equilibrium model. The Park model without finite rate sublimation experiences a sharp dropoff at 54 s, indicating that sublimation must remain in the reaction set for nonequilibrium trends to be comparable to equilibrium.

V. Comparison to Other Nonequilibrium Stardust Models and Reentry Flight-Test Data

A. Computational Models

Adequate arcjet test data were not available for the present work [3,19]. Thus, the results of this study were compared against those of Chen and Milos [8]. Chen and Milos used an iteration scheme [Eq. (7)] to solve for surface conditions, which is different from the Newton–Raphson method used in MAT. The previous work calculated parameters such as heat flux directly from their iterative approach, whereas the MAT/FIAT setup has MAT compute surface chemistry conditions that FIAT draws upon to find heat fluxes and mass flux. Chen and Milos [8] described the four reactions of the Park finite rate model as the only reactions occurring on the surface, focused on convection and ablation rates, and used a simplified energy balance equation to predict convection:

$$q_{\text{conv}} = \sigma\varepsilon T_w^4 + \dot{m}h_w^{\text{gas}} \tag{19}$$

Table 1 Total blowing rates and convective heat flux for two approaches to Stardust at peak heating

Approach	Total ablation rate, kg/m^2s	Convective heat flux, W/cm^2
Chen and Milos (approximate) [8]		
Chemical equilibrium [10]	0.090	700
Park (nitridation) [8]	0.095	500
Park (no nitridation) [8]	0.058	530
MAT/FIAT		
Chemical equilibrium [10]	0.088	590
Park (nitridation) [8]	0.054	450
Park (no nitridation) [8]	0.054	450
Park (no sublimation) [8]	0.054	410

Table 1 compares the present results for the convective heating results and total ablation rates at the stagnation point at 54 s with those of [8]. The present work includes more factors on the surface, as FIAT uses radiation across the surface, conduction, and chemical contributions when computing surface heat fluxes [8]. In the implementation of the Park finite rate model in [8], Chen and Milos found that the total ablation rate decreased when nitridation was eliminated from the Park model. There is a similar reduction in the total ablation rate for finite rate nonequilibrium when MAT and FIAT are used, except that the reduction is found for all nonequilibrium reaction sets. Including nitridation resulted in an increase of 63% of the total ablation rate compared with leaving nitridation absent from the reaction set and a 5.6% increase over the chemical equilibrium assumption. With MAT/FIAT there is no significant difference in the total ablation rate or convective heat flux between a reaction set with or without nitridation.

All nonequilibrium implementations reduced the convective heat flux, though there are differing reasons as to why the present model and the model of Chen and Milos predict a decrease. The differences in the convective heat flux seen in Table 1 due to nonequilibrium in [8] may be caused by the omission of nitrogen and oxygen recombination at the surface. The lower convective heat flux with the nonequilibrium FIAT/MAT may be due to extending the model over the entire trajectory, using more energy considerations in the energy balance equation, and changing material properties as ablation occurred. Additionally, oxygen and nitrogen recombination are considered to be in equilibrium for FIAT/MAT. There is no significant change in the net convective heat flux due to nitridation seen by FIAT or the previous work. Chen and Milos [8] explained that the Park finite rate model with nitridation has a slightly lower convective heat flux than the model without nitridation because the nitridation reaction significantly increased the ablation rate, but released only a small amount of energy.

Chen and Milos [8] previously compared their nonequilibrium convective heat flux, computed using a simplified surface energy balance, with Park's convective heat flux without radiation. Although there was some agreement between the two data sets, the same comparison is not rigorously made here, as radiation is not simplified in FIAT. Park compared his heat transfer results with radiation with those from Olynick without ablation assuming that the surface temperature remains at 3000 K. The total heating rates from Park [7] with laminar flow, Olynick et al. [9] (no ablation), the FIAT equilibrium, and the present work are shown in Fig. 10. Park's results were greater than those found by FIAT for the ablating case and were closer to those of Olynick et al. for a nonablating material. The heating rates for the Park nonequilibrium model in the present work are closer to the FIAT equilibrium values than Park's independently calculated values for a similar set of reactions. Because Park validated the ablating heating rates against those of Olynick et al. without ablation, a comparison between the results found by the use of nonequilibrium and those in [7] would be of limited value.

B. Comparison to Stardust Flight-Test Data

Because the temperatures were optically measured during the SRC reentry and averaged over the entire heat shield, they cannot be compared with the computed stagnation point surface temperature [13,28]. Initial equilibrium calculations by Olynick et al. [9] and Chen and Milos [10] predicted a recession near 1 cm at the stagnation point. During postflight analysis [14], the equilibrium stagnation point recession was computed as 1.04 cm using a new PICA model. The original equilibrium FIAT model overpredicted the recession not only at the stagnation point but also at all points of interest [14]. Recession could not be measured at the stagnation point of the recovered SRC; however, the near-stagnation point on the heat shield was measured to have receded 0.57 cm, with a $\pm 3\%$ error in the

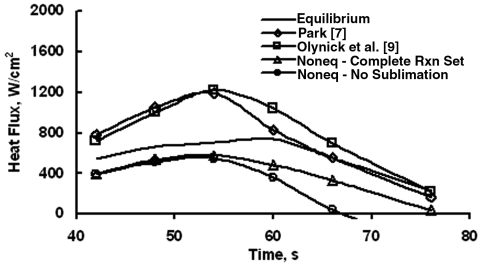

Fig. 10 Predicted total heating flux for various models.

measurement. The equilibrium stagnation point recession was computed as 1.12 cm in this current work.

The inclusion of four finite rate reactions (sublimation, two oxidation, and nitridation) to account for the nonequilibrium surface conditions in the present work led to a reduction in the predicted recession of 36%, from 1.12 to 0.72 cm. If the stagnation point recession had the same discrepancy (61% overprediction) as the near-stagnation point, the stagnation point recession calculation of Stackpoole et al. [14] (1.04 cm) leads to an assumed actual recession of 0.65 cm at the stagnation point. The full reaction set nonequilibrium recession of 0.72 still overpredicted the recession, but now only by 11%. When nitridation and sublimation were omitted from the Park model and allowed to reach equilibrium, the predicted recession was 0.49 cm, underpredicting the measured recession by 25%.

VI. Conclusions

An investigation into nonequilibrium surface interactions during Stardust reentry for the heat shield material PICA has been conducted. Previously, nonequilibrium surface conditions were studied for a PICA material under Stardust reentry conditions, but only at a few trajectory points [8,10]. These investigations were not coupled with a detailed material response. In the present work, Park's method for nonequilibrium surface reactions is integrated into the surface chemistry program MAT to allow for both equilibrium and nonequilibrium conditions. MAT was chosen primarily because it had previously been able to calculate nonequilibrium surface conditions. MAT was then loosely coupled to FIAT such that a completed material response could be modeled for a full SRC reentry trajectory.

A full Park finite rate model reaction set and a set without nitridation and sublimation to simulate surface nonequilibrium were studied. It was assumed that the reactions not accounted for in the Park model reached equilibrium. For the full reaction set, nonequilibrium slightly decreased the temperature on the surface. The char ablation rate, the convective heat flux, and the heat loads decreased due to the nonequilibrium conditions. It was shown that the decrease in the heat flux was due in part to the increase in the wall enthalpy, which offset the decreased total ablation rate. The computed recession using a full reaction set Park finite rate model was closer to the recession that was measured from the actual Stardust reentry; the measured recession at the stagnation point was extrapolated from the measured recession at the near-stagnation core. The recession previously predicted with equilibrium conditions overpredicted the recession data by more than 50%.

The Park finite rate model showed that sublimation plays a key role when assuming finite rate nonequilibrium. Sublimation was allowed to reach full equilibrium by removing it from the Park model. Without sublimation, the calculations of the temperature and char ablation rate after the surface reached 3000 K did not match previous nonequilibrium modeling or flight data. Because of the absence of finite rate sublimation, the surface cooled quickly and the char ablation rate approached zero more rapidly than in equilibrium. Additionally, predicted recession was below the actual measured value. In future work, the application of the Park finite rate model to more locations on the SRC heat shield would permit a comparison with the optically derived flight data. Validated arcjet test data for PICA would also provide further validation of the computational model presented here.

Acknowledgments

The authors wish to thank the support and funding of the Space Vehicle Technology Institute, one of the NASA Constellation University Institute Projects (CUIP), under grant NCC3-989, with joint sponsorship from the U.S. Department of Defense. Thanks go to Claudia Meyer of the NASA John H. Glenn Research Center at Lewis Field, program manager of CUIP, and to John Schmisseur of the U.S. Air Force Office of Scientific Research. The help provided by Frank S. Milos and Thomas H. Squire of NASA Ames Research Center in the understanding of the FIAT code, David G. Drewry of Johns Hopkins University Applied Physics Laboratory in material response expertise, and Bernard Laub in the preliminary review of the results is also greatly appreciated.

References

[1] Viviani, A., Pezzella, G., and Borrelli, S., "Effect of Finite Rate Chemical Models on the Aerothermodynamics of Reentry Capsules," AIAA Paper 2008-2668, April 2008.

[2] Park, C., and Tauber, M. E., "Heatshielding Problem of Planetary Entry, A Review," AIAA Paper 99-33601, June 1999.

[3] Tran, H. K., Johnson, C. E., Rasky, D. J., Hui, F. C. L., Hsu, M.-T., Chem, H. C., and Chen, Y. K., "Phenolic Impregnated Carbon Ablators (PICA) for Discovery Class Missions," AIAA Paper 96-1911, June 1996.

[4] Kontinos, D., and Stackpoole, M., "Post-Flight Analysis of the Stardust Sample Return Capsule Earth Entry," AIAA Paper 2008-1197, Jan. 2008.

[5] Beerman, A. F., Lewis, M. J., Starkey, R. P., and Cybyk, B. Z., "Nonequilibrium Surface Interactions Ablation Modeling with the Fully Implicit Ablation and Thermal Response Program," AIAA Paper 2008-1224, Jan. 2008.

[6] Park, C., and Ahn, H. K., "Stagnation-Point Heat Transfer Rates for Pioneer-Venus Probes," *Journal of Thermophysics and Heat Transfer*, Vol. 13, No. 1, Jan.–March 1999, pp. 33–41. doi:10.2514/2.6426

[7] Park, C., "Calculation of Stagnation-Point Heating Rates Associated with Stardust Vehicle," *Journal of Spacecraft and Rockets*, Vol. 44, No. 1, Jan.–Feb. 2007, pp. 24–32. doi:10.2514/1.15745

[8] Chen, Y. K., and Milos, F. S., "Finite-Rate Ablation Boundary Conditions for a Carbon-Phenolic Heat-Shield," AIAA Paper 2004-2270, June 2004.

[9] Olynick, D., Chen, Y. K., and Tauber, M. E., "Aerothermodynamics of the Stardust Sample Return Capsule," *Journal of Spacecraft and Rockets*, Vol. 36, No. 3, May–June 1999, pp. 442–462. doi:10.2514/2.3466

[10] Chen, Y. K., and Milos, F. S., "Ablation and Thermal Response Program for Spacecraft Heatshield Analysis," *Journal of Spacecraft and Rockets*, Vol. 36, No. 3, May–June 1999, pp. 475–483. doi:10.2514/2.3469

[11] Milos, F. S., and Chen, Y. K., "Comprehensive Model for Multicomponent Ablation Thermochemistry," AIAA Paper 97-0141, Jan. 1997.

[12] "Stardust Hypervelocity Entry Observing Campaign Support," NASA Engineering and Safety Center Rept. RP-06-80, 31 Aug. 2006.

[13] Jenniskens, P., "Observations of the STARDUST Sample Return Capsule Entry with a Slit-Less Echelle Spectrograph," AIAA Paper 2008-1210, Jan. 2008.

[14] Stackpoole, M., Sepka, S., Cozmuta, I., and Kontinos, D., "Post-Flight Evaluation of Stardust Sample Return Capsule Forebody Heatshield Material," AIAA Paper 2008-1202, Jan. 2008.

[15] Koo, J. H., Ho, D. W. H., and Ezekoye, O. A., "A Review of Numerical and Experimental Characterization of Thermal Protection Materials—Part I. Numerical Modeling," AIAA Paper 2006-4936, July 2006.

[16] Park, C., Jaffe, R. L., and Partridge, H., "Chemical-Kinetic Parameters of Hyperbolic Earth Entry," *Journal of Thermophysics and Heat Transfer*, Vol. 15, No. 1, Jan.–March 2001, pp. 76–90. doi:10.2514/2.6582

[17] Milos, F. S., and Rasky, D. J., "Review of Numerical Procedures for Computational Surface Thermochemistry," *Journal of Thermophysics and Heat Transfer*, Vol. 8, No. 1, 1994, pp. 24–34. doi:10.2514/3.497

[18] Dolton, T. A., Maurer, R. E., and Goldstein, H. E., "Thermodynamic Performance of Carbon in Hyperthermal Environments," AIAA Paper 68-754, June 1968.

[19] Covington, M. A., Heinemann, J. M., Goldstein, H. E., Chen, Y. K., Terrazas-Salinas, I., Balboni, J. J., Olejniczak, J., and Martinez, E. R., "Performance of a Low Density Ablative Heat Shield Material," *Journal of Spacecraft and Rockets*, Vol. 45, No. 2, March–April 2008, pp. 237–247.
doi:10.2514/1.12403

[20] Park, C., "Stagnation-Point Ablation of Carbonaceous Flat Disks–Part I: Theory," *AIAA Journal*, Vol. 21, No. 11, Nov. 1983, pp. 1588–1594.
doi:10.2514/3.8293

[21] Dec, J. A., and Braun, R. D., "An Approximate Ablative Thermal Protection System Sizing Tool for Entry System Design," AIAA Paper 2006-780, Jan. 2006.

[22] "User's Manual: Aerotherm Charring Material Thermal Response and Ablation Program," Aerotherm Div., Acurex Corp., Mountain View, CA, Aug. 1987.

[23] Park, C., "Effects of Atomic Oxygen on Graphite Ablation," *AIAA Journal*, Vol. 14, No. 11, Nov. 1976, pp. 1640–1642.
doi:10.2514/3.7267

[24] Scala, S. M., "The Ablation of Graphite in Dissociated Air, I. Theory," General Electric, Missile and Space Division R62SD72, Sept. 1962.

[25] Milos, F. S., and Marschall, J., "Thermochemical Ablation Model for TPS Materials with Multiple Surface Constituents," AIAA Paper 94-2042, June 1994.

[26] Bartlett, E. P., Kendall, R. M., and Rindal, R. A., "An Analysis of the Chemically Reacting Boundary Layer and Charring Ablator. Part IV: A Unified Approximation for Mixture Transport Properties for Multicomponent Boundary-Layer Applications," NASA CR-1063, June 1968.

[27] Bianchi, D., Martelli, E., and Onofri, M., "Practical Navier–Stokes Computation of Flowfields with Ablation Products Injection," ESA SP-631, June 2006.

[28] Trumble, K. A., Cozmuta, I., Sepka, S., and Jenniskens, P., "Post-Flight Aerothermal Analysis of the Stardust Sample Return Capsule," AIAA Paper 2008-1201, Jan. 2008.